Photorealistic Rendering of Human Hair Fibers

Iman Sadeghi*
M.Sc. Thesis in Computer Science and Engineering
University of California, San Diego

Our rendering results for rendering different hair colors using different shading models. (Right) Model of Kajiya and Kay. (Center) Model of Marschner et al. (left) Generalized model of Zinke with multiple scattering. Hair models are courtesy of Walt Disney Animation Studios.

Abstract

Photorealistic rendering of human hair has been a challenge task in computer graphics for many years. These challenges include coming up with a practical yet accurate light scattering model for individual hair fibers, handling the complex geometry of large number of hair fibers, properly simulating the global illumination and complex interaction of light and shadows between the hair strands, and overcoming aliasing problems due to the fine geometry of the hairs. In this paper, we present an overview of the physical and optical properties of human hair fibers, investigate the most prominent hair shading models, and at the end we critically analyze each shading model. We also briefly go over the approaches for simulating multiple scattering of light in hair rendering. We have implemented all of the shading models which have been discussed in the paper and we will discuss their strengths and weaknesses in detail. Furthermore, we discuss missing behaviors in current shading models compared to the experimental measurements and propose possible avenues of future research.

CR Categories: I.3.7 [Computer Graphics]: Three-Dimensional Graphics and Realism—Color, shading, shadowing, and texture

Keywords: hair, rendering, shading model, light scattering, multiple scattering

1 Introduction

Generally, hair simulation in computer graphics can be divided into three main categories: hair styling, hair simulation, and hair rendering. Hair styling is the process of defining the 3D geometry of hair strands and usually requires specifying the orientation, distribution and density of the hair fibers. Hair simulation is the process of animating the motion of the hair strands. Dynamics of hair movements, collision detection, and simulation of internal interactions between hair strands is essential for accurately animating the hair. Hair rendering, which is the topic of this paper, is the process of synthesizing 2D images from an underlying mathematical presentation of hair strands. Research in hair rendering includes the following: deriving practical and accurate light scattering models for determining the appearance of assembly of hair fibers; simulating the multiple scattering and global illumination effects; computing shadows inside the hair volume; and overcoming the aliasing problems due to the fine geometry of hair strands. Also, interactive rendering and acceleration techniques for hair rendering has attracted a lot of attention recently. Each mentioned subcategory faces a lot of challenging problems and is being actively researched.

Our main focus in this paper is to give a comprehensive overview of different light scattering models that are currently being used in the computer graphics community. Also, we will briefly go over the attempts for simulating multiple scattering in hair rendering. We begin by pointing out the notations used for describing the geometry of light scattering from fibers which will be used throughout the paper in Section 2. In Section 3, we will present an overview of the physical and optical properties of human hair fibers. In Section 4, we present the principals of light scattering form smooth cylinder which is the basis of all hair rendering models.

We proceed by investigating the most prominent hair shading models in Section 5. Discussed models include the classical hair shading model of Kajiya and Kay [1989], improved shading models of Goldman [1997] and Kim [2002], physically based model of Marschner et al. [2003], and Zinke's generalized shading model [2004; 2007]. In Section 6, we summarize the attempts in simulating the global illumination and multiple scattering effect in the context of hair rendering. These approaches include Monte Carlo based models [Moon and Marschner 2006; Zinke and Weber 2006], photon mapping based models [Moon and Marschner 2006; Zinke and Weber 2006], and approximation approaches [Zinke et al. 2008]. We continue by critically analyzing each shading model in Section 7. We will point out the strengths and weaknesses of each shading model in detail and compare their rendering results. In Section 8,

*e-mail: iman@graphics.ucsd.edu

we mention missing behaviors in current shading models by comparing them to experimental measurements, and propose possible avenues for future research.

2 Notation and Radiometry of Fibers

This section summarizes the notations used throughout the paper. These notations are mainly taken from the works by Marschner et al. [2003] and Zinke et al. [2007]. Other models will be stated according to these notations in order to ease the comparison process. Most of the published literature in rendering hair does not discuss the radiometry of hair fibers but here we present a formalized description of curve scattering function which has been mainly introduced by Marschner et al. [2003].

2.1 Scattering Geometry Notations

We treat fiber geometries as 3D elliptical cylinders. The tangent direction of a hair fiber is shown by vector $\vec{u}$ which points toward the tip of the hair. The plane perpendicular to this direction is referred to as the *normal plane*. The direction parallel to the major axis of the elliptical cross section of the cylinder is denoted by $\vec{v}$ and the minor axis is $\vec{w}$. The direction of illumination is ω_i and the viewing direction or the direction in which the scattered light is being measured is ω_r. Both the viewing direction and the illumination direction vectors point away from the center point. For parameterizing ω_i and ω_r we use spherical coordinates. The inclinations of ω_i and ω_r with the normal plane are referred to as θ_i and θ_r respectively. All directions with $\theta = 0$ lie on the normal plane, $\theta = \frac{\pi}{2}$ is $\vec{u}$ and $\theta = -\frac{\pi}{2}$ is $-\vec{u}$. The azimuthal angles of ω_i and ω_r around hair are denoted by ϕ_i and ϕ_r respectively. $\phi = 0$ is equal to $\vec{v}$ and $\phi = \frac{\pi}{2}$ equals $\vec{w}$. The relative azimuthal angle $\phi_r - \phi_i$ is denoted as ϕ, and the half azimuthal angle $\frac{\phi_r+\phi_i}{2}$ is denoted as ϕ_h. Similarly, the half longitudinal angle θ_h and relative longitudinal angle $\Delta\theta$ are defined as $\frac{\theta_r+\theta_i}{2}$ and $\frac{\theta_r-\theta_i}{2}$ respectively. The refracted longitudinal angle inside the hair fiber is refereed to as θ_t. All mentioned geometry notations of light scattering from fibers are summarized in Figure 1.

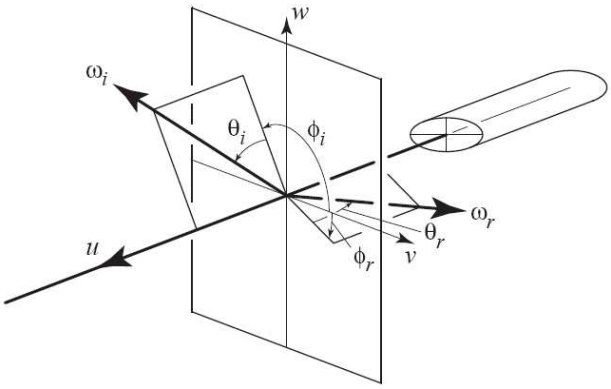

Figure 1: *Macroscale geometry notations for light scattering form fibers. From [Marschner et al. 2003].*

There are two other notations which will be useful when one wants to take into account the microscale geometry of light scattering in hair fibers: the azimuthal offset h and the longitudinal offset s. The value of the azimuthal offset is the distance of the intersecting ray to a parallel vector which goes through the center of the fiber. The absolute range of azimuthal offsets is less than the radius of the fiber (see Figure 2). The value of the longitudinal offset is the distance that light transports inside the hair fiber along the $\vec{u}$ direction. These offset notations are taken from the works by Zinke et al. [2004; 2007] and later will be used to describe their proposed models.

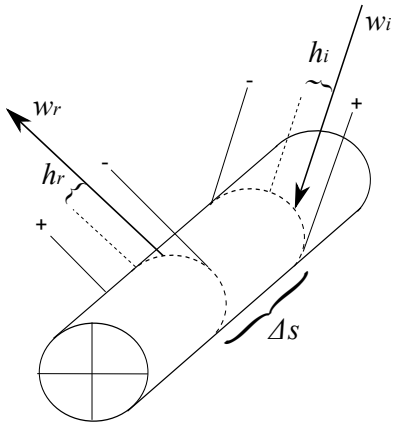

Figure 2: *Microscale geometry notations for light scattering form fibers*

2.2 Radiometry of Fiber Reflection

Hair fibers can be treated as simple 1D entities. Therefore, the description of light scattering from hair fibers should be described in a different manner than the usual light scattering parameters for surface reflection. For 2D surfaces, we can define the light scattering behavior as the conventional bidirectional reflectance distribution function, $f_r(\omega_i, \omega_r)$, or in short BRDF. The BRDF describes the distribution density of the scattered flux with respect to the projected solid angle in direction ω_r relative to the incident light beam from direction ω_i.

The bidirectional reflectance distribution function is defined to be the ratio of the surface radiance exiting the surface in direction ω_r to surface irradiance falling on the surface from a differential solid angle in the direction ω_i:

$$f_r(\omega_i, \omega_r) = \frac{dL_r(\omega_r)}{dE_i(\omega_i)} \tag{1}$$

Therefore, the scattered radiance due to an incident radiance distribution $L_i(\omega_i)$ is calculated by the following integral over all possible incoming directions for ω_i on a hemisphere H^2:

$$L_r(\omega_r) \;=\; \int_{H^2} f_r(\omega_i, \omega_r)\; L_i(\omega_i) \cos\theta_i \; d\omega_i \tag{2}$$

Similarly, we can define the light scattering from fibers $f_s(\omega_i, \omega_r)$ by defining the *curve radiance*, L_r^c, and *curve irradiance*, E_i^c. Curve radiance and curve irradiance are similar to the conventional radiance and irradiance but with different units. Curve radiance is defined as power per projected length per solid angle and curve irradiance is defined as power per unit length. Consequently, the *curve scattering function* f_s is the ratio of curve radiance exiting the curve in direction ω_r to curve irradiance falling on the curve from a differential solid angle in the direction ω_i:

$$f_s(\omega_i, \omega_r) = \frac{dL_r^c(\omega_r)}{dE_i^c(\omega_i)} \tag{3}$$

Thus, the outgoing curve radiance L_r^c, due to illumination from an incoming radiance distribution L_i, would be computed as the following integral over all possible directions for ω_i on a whole sphere S^2:

$$L_r^c(\omega_r) \;=\; D \int_{S^2} f_s(\omega_i, \omega_r)\, L_i(\omega_i) \cos\theta_i \, d\omega_i \qquad (4)$$

In the above integral, D is the diameter of the hair as seen from the illumination direction (note that D is not necessarily constant and is a function of ϕ_i for elliptical fibers). This shows that although identical fibers of different widths have the same scattering function, thick fibers intercept more light than thin fibers and therefore look brighter.

Curve radiance and curve irradiance were first introduced to the graphics community by Marschner et al. [2003]. These curve (1D) radiometry parameters are midway between surface (2D) radiometry and particles (0D) radiometry.

3 Physical Measurements of Human Hair Fibers

Any hair rendering system needs a model for predicting the scattering of light from hair fibers. This scattering model is similar to the local illumination model in conventional surface rendering systems. This section summarizes the studied physical properties of human hair fibers in literature and focuses on the measurements of optical properties of the human hair fibers.

3.1 Physical Properties of Hair Fibers

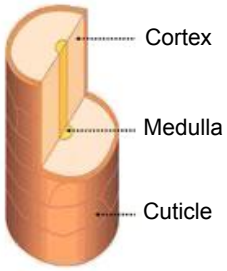

Figure 3: *The structure of human hair fibers. From* `http://www.hoyu-usa.com`.

The human hair fiber consists of three main components: the cortex, the cuticle and the medulla (see Figure 3). The cortex is the main part of the hair fiber and gives hair its physical strength. The cuticle covers the surface of the fiber and has the role of protection for the inner cortex. The cuticle is the main interface of hair with air and so it is mainly responsible for the behavior of light scattering by the fiber. This thin layer is composed of flat cells that overlap on top of each other and has a structure like roof shingles [Marschner et al. 2003]. On the microscopic levels the surface of hair fiber appears as a nested set of cones (see Figure 4). This overlapping structure causes the fiber's surface normals to be slightly away from the expected normal direction. Experiments have shown that these tilted cells shift the normal of the surface toward the root of the fiber by approximately five degrees [Bustard and Smith 1991; Robbins 1994]. The medulla sometimes exists near the axis of the hair and its functionality is still unknown. The medulla and cortex contain pigments that absorb different amounts of light with different wavelengths and together they cause the coloration of hair fibers. As observed by Robbins, the cross section of hair fibers can vary from circular to elliptical to irregular [Robbins 1994]. He has also reported that hair is composed of amorphous protein which acts as transparent medium with index of refraction $\eta = 1.55$.

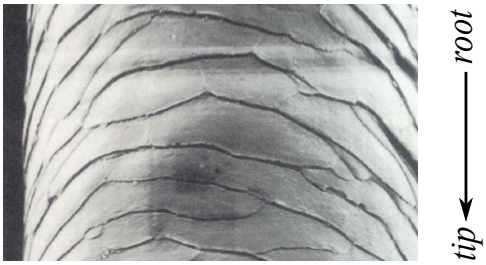

Figure 4: *An electron micrograph of a hair fiber which shows the structure of the cuticle layer. In this image the fiber is oriented with the root at the top and the tip at the bottom. From [Robbins 1994].*

3.2 Light Scattering Properties of Hair Fibers

There have been many measurements of light scattering from human hair fibers. Stamm et al. [1977] and Bustard and Smith [1991] conducted experiments for measuring the scattering of light in the *incident plane* (where light and eye directions are coplanar with the fiber axis) of the hair fibers. Their main goal was to understand the properties that makes the hair look pleasing and healthy. Marschner et al. [2003] went beyond these measurements and examined out-of-plane light scattering of hair fibers using a 3D goniophotometer.

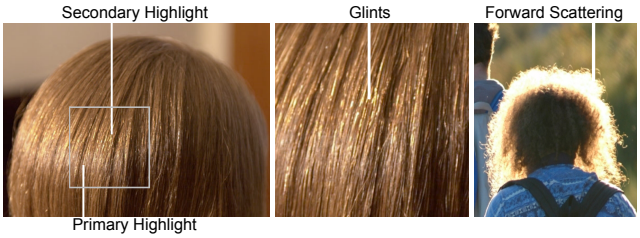

Figure 6: *Real hair appearance. (left) The appearance of primary and secondary highlight in brown hair. (center) Glints give hair its textured appearance. From [Marschner 2005] (right) Forward scattering that exist in the case of back-lighting. From [Zinke 2007].*

Stamm et al. [1977] made measurements of light scattering from arrays of parallel fibers. They measured relative scattering of light by the fibers as a function of illumination and viewing angles in the incident plane.

In their experiments, they observed two surprising behaviors. The first observation is that the angle of the primary specular highlight peak deviates several degrees away from the mirror specular direction. The second observation was that there is a secondary highlight peak which appears on the other side of the mirror specular direction. They also observed that at the grazing angles there is a sharp specular highlight that lies on the mirror reflection [Stamm et al. 1977].

They speculated that the source of these shifts in reflection angles is due to the effect of tilted scales of the cuticle layer. The first specular highlight is reflected from the surface of the fiber and the second highlight is the result of internal reflection of light form the back side of the fiber (i.e. light which has been refracted, reflected

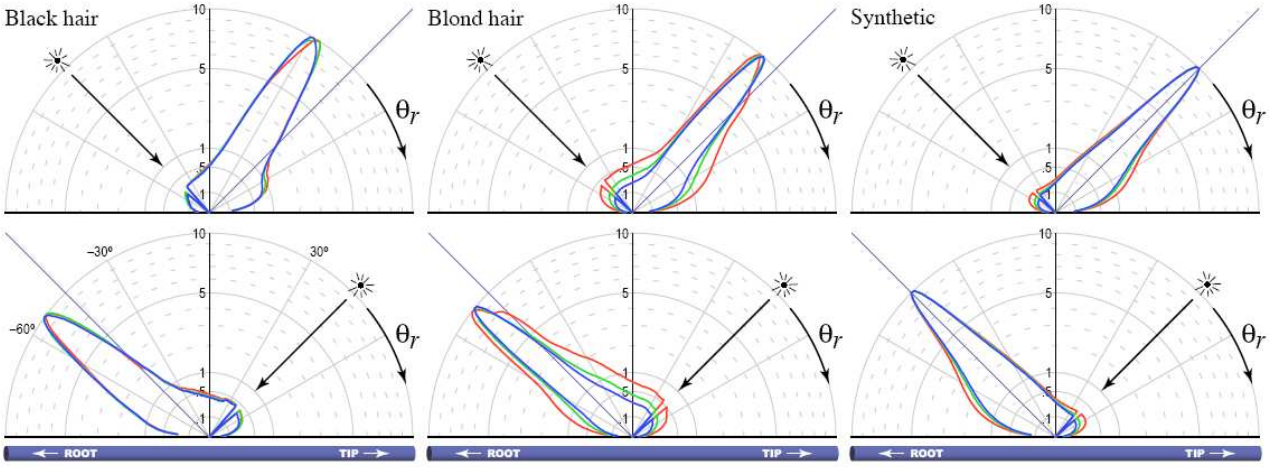

Figure 5: *Measurements of scattering in the incident plane: scattering as a function of scattering angle with illumination at 45^o from the tip and root ends. Black and blond hair are shown, along with a synthetic fiber from a wig. From [Marschner et al. 2003]*

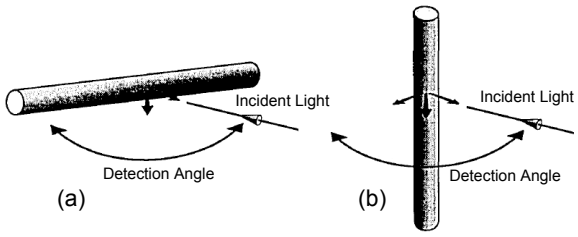

Figure 7: *Bustard and Smith setup. (a) Incident plane measurements. (b) Normal plane measurements. From [Bustard and Smith 1991].*

and again refracted). According to their observation, the first highlight is not colored whereas the second highlight is colored. Bustard and Smith [1991] later reported that first highlight preserves polarization but the second highlight is depolarized. Additionally, black hair only shows the first highlight peak [Stamm et al. 1977; Bustard and Smith 1991]. These experiments are along with the explanation that the first highlight is the single reflection off the surface and that the second highlight is the internal reflection of light.

Bustard and Smith [1991] had some preliminary reports where they experimented with azimuthal scattering of light in the normal plane of the fiber and they observed some sharp peaks. They speculated that those sharp peaks can be the result of internal caustics. However, they did not report any data on their conjecture.

Stamm et al.'s and Bustard and Smith's measurements were in the incident plane and so their report only shows a 2D slice of the whole 3D scattering function. Marschner et al. [2003] extended the measurements over these 2D measurements and reported a more complete set of light scattering measurements for light scattering by a single hair fiber. In addition to the incident plane measurements, which was in agreement with Stamm and Bustard results, they have reported normal plane measurements which capture the details of those sharp peaks observed by Bustard and Smith. Authors plotted the behavior of those sharp peaks as the strand of hair rotates around its axis. They named these sharp peaks as glints and showed that the behavior of the glints match a Monte Carlo simulation of light scattering by an elliptical cylinder. This confirms that glints are actually formed by internal caustics inside the hair fiber (see

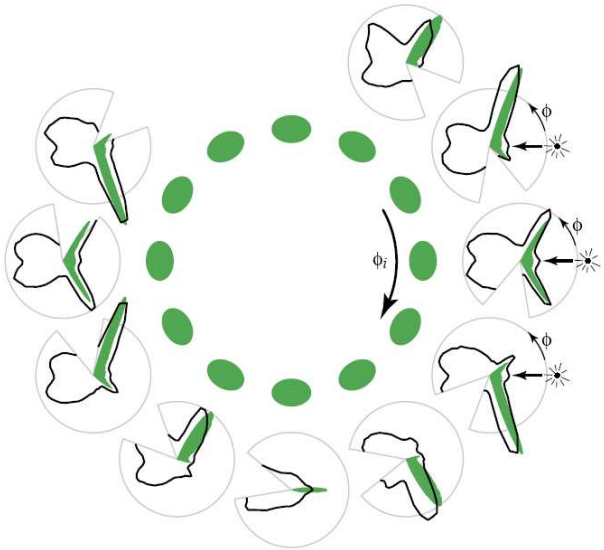

Figure 8: *Black solid lines show the measurement of light scattering in the normal plane for a blond hair with elliptical cross section. Green ellipses in the middle show the orientation of hair. Location and strength of the glints depend on the orientation of the fiber. The green plots are the results of Monte Carlo scattering simulation and they match the measured results qualitatively. From [Marschner et al. 2003].*

Figure 8). Marschner et al. [2003] additionally present hemispherical measurements that show the evolution of different highlights with respect to changes in relative azimuthal angle, which showed the full light scattering distribution for a fixed incident angle (see Figure 9).

4 Principles of Light Scattering from Cylinders

This section discusses the theoretical background on studying the reflection of light from smooth cylinders. These theories are impor-

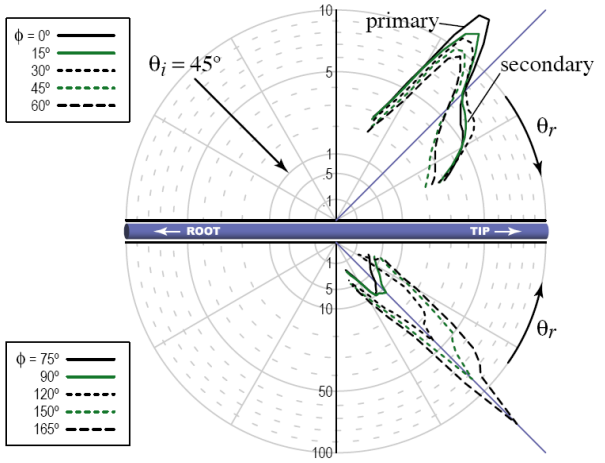

Figure 9: *Hemispherical measurements of Marschner et al. The incident direction is fixed with angle of incidence 45^o. The primary highlight, secondary highlight and forward scattering component have been plotted for different relative azimuthal angles. From [Marschner et al. 2003].*

tant particularly because most of the shading models are based on the assumption that the fibers are perfect smooth cylinders and then they add some controlling parameters (sometimes physically based and sometimes ad hoc) to change the behavior of their model. There have been thorough studies on the properties of light-scattering from cylinders in order to determine the properties of optical fibers [Marcuse 1974; Adler and Stone 1998; Mount and Marston 1998]. In the rest of this section, we mention the properties of cylinder optics which enable us to factor the general 4D scattering function $f_s(\phi_i, \theta_i; \phi_r, \theta_r)$ into the product of two 2D functions. We use the notations introduced by Marschner et al. [2003] and use $M(\theta_i, \theta_r)$ and $N(\phi_i, \phi_r)$ for the longitudinal and azimuthal components respectively.

The most important property in this topic is the one that was first introduced to the graphics community by Kajiya and Kay [1989]. Kajiya and Kay pointed out that the specular reflection of a parallel bundle of rays off a cylinder would lie inside a cone with apex angle equal to the incident angle. For an intuitive proof consider the intersection of a parallel beam of light with a cylinder. Since normals on the cylinder point in all directions inside the normal plane, the reflected light is independent of the azimuthal angle of the incident direction. As a result, all the reflected rays will make the same angle with the normal plane and hence lie on a cone centered at the hair fiber. For a more mathematical proof of this fact see Appendix A.

Consequently, we have the following rule of thumb: when a ray enters a dielectric cylinder it will exit with the same longitudinal inclination as the incident beam no matter how many times it has been reflected/refracted inside the cylinder. Note that this property itself reduces the 4D scattering function $f_s(\phi_i, \theta_i; \phi_r, \theta_r)$ to a 3D scattering function $f_s(\phi_i, \theta_i, \phi_r)$ since we always have $\theta_r = -\theta_i$.

Besides, according to Bravais law (Appendix B), if one projects the incident and transmitted rays onto a plane which contains the surface normal, the projected vectors will still obey the Snell's law and Fresnel attenuation formulas. However, the effective index of refraction, η', would be different than the actual index of refraction, η, and is a function of inclination angle. For Snell's law, it is sufficient to use η' and for the Fresnel calculations one should use η' for the perpendicular component of the reflectance and η'' for the parallel component. Where η' and η'' can be derived according to the following expressions: (Refer to Appendix B for more discussion)

$$\eta'(\theta_i) = \frac{\sqrt{\eta^2 - \sin^2\theta_i}}{\cos\theta_i} \quad (5)$$

$$\eta''(\theta_i) = \frac{\eta^2 \cos\theta_i}{\sqrt{\eta^2 - \sin^2\theta_i}} = \frac{\eta^2}{\eta'(\theta_i)} \quad (6)$$

Therefore, in order to compute the scattering function for any fibers with fixed cross section one can decompose the computations of a 4D scattering function $f_s(\phi_i, \theta_i; \phi_r)$ to the product of two 2D functions $N(\phi_i, \phi_r, \eta')$, the azimuthal scattering function, and $M(\theta_i, \theta_r)$, the longitudinal scattering function. Note that this is decomposing the calculations and not decomposing the actual scattering function since η' is itself function of θ_i. Thus, any light scattering model for cylindrical fibers can be stated as:[1]

$$f_s(\phi_i, \theta_i; \phi_r, \theta_r) = M(\theta_i, \theta_r) \times N(\phi_i, \phi_r, \eta') \quad (7)$$

Note that in case of perfect smooth cylinders $M(\theta_i, \theta_r)$ component further reduces to a 1D function $M(\theta_i)$ since $\theta_i = -\theta_r$.

At the end, the main difference between the proposed shading models boils down to the definition of their azimuthal scattering functions N. For a perfect circular cross section, N only depends on ϕ and so the 2D azimuthal scattering function reduces to a 1D function. Marschner et al. [2003] analytically derived the exitant intensity distribution of the incident beam of light for perfect circular cross sections. If we consider that the incident beam of light comes from a small interval dh and after scattering it spreads into an angular interval $d\phi$ (see Figure 10), then we can abstractly refer to the exitant intensity distribution as:

$$\overline{L}(\phi(h)) = \overline{E}/|2\frac{d\phi}{dh}| \quad (8)$$

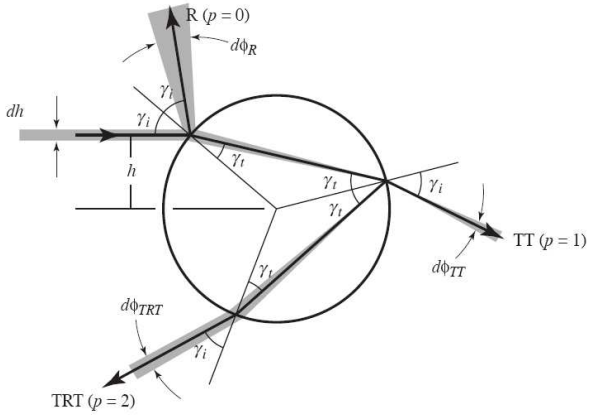

Figure 10: *Geometry for scattering from a circular cross section. $d\phi/dh$ represents the focusing and dispersion of light. From [Marschner et al. 2003].*

[1] Please note that we are using a slightly different notation than Marschner et al. [2003] since we are migrating the $1/\cos\theta_d^2$ term into the longitudinal scattering function.

where attenuation is not taken into account and $\overline{E} = 2E(h_i)$ is the uniform irradiance which falls on the cross section of the fiber. For more discussion and practical ways of calculating this exitant intensity distribution for perfect circular cross sections refer to the work by Marschner et al. [2003].

5 Shading Models for Hair Rendering

Given an incident light directions, a hair shading model states how much a hair fiber scatters light into an outgoing directions. In this section we will mention different prominent shading models chronologically and discuss their strength and weaknesses.

5.1 Kajiya and Kay 1989

The earliest and most widely used model for rendering hair fibers is Kajiya and Kay's model which was originally developed for rendering fur [Kajiya and Kay 1989] but has been used in rendering hair in general extensively. Their model is very simple and captures the most important visual feature of light scattering from fibers which is the anisotropic reflection of light by hair fibers which we have referred to it earlier in the text as the primary highlight.

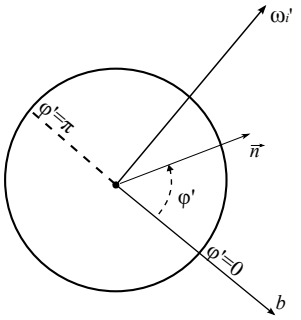

Figure 11: *Derivation of Kajiya and Kay's diffuse component.*

Kajiya and Kay's model is composed of two components: a diffuse component and a specular component. The diffuse component of their reflection model is obtained by integrating over a Lambert reflection model along the circumference of the half cylinder which faces the light source. For the calculations, they set up an orthogonal basis from three vectors u, ω_i' and b where u is the direction of the hair fiber, ω_i' is the projection of ω_i on the normal plane and b is the cross product of ω_i' and u. The total amount of light scattered per unit length of cylinder is integrated over the semicircle from shadow terminator to shadow terminator (see Figure 11). By parameterizing the position along the cylinder by angle φ' where φ' ranges between 0 and π radians the normal vector $\vec{n}$ is defined by the following expression:

$$\vec{n} = b(\cos\varphi') + \omega_i'(\sin\varphi') \tag{9}$$

The Lambertian intensity is given by $\Psi^{Lambert}(\varphi') = k_d\omega_i.n$ and by integrating it along the circumference of the cylinder we get the total amount of diffuse light per unit length.

$$\begin{aligned}
\Psi^{K\&K}_{Diffuse} &= k_d \int_0^{\pi} \omega_i \,.\, n\, r\, d\varphi' \\
&= k_d\, r \int_0^{\pi} \omega_i \,.\, (b(\cos\varphi') + \omega_i'(\sin\varphi'))\, d\varphi' \\
&= k_d\, r\omega_i \,.\, \omega_i' \int_0^{\pi} \sin\varphi' d\varphi' \\
&= 2\, k_d\, r\, \omega_i \,.\, \omega_i' \\
&= K_d\, \cos\theta_i
\end{aligned} \tag{10}$$

For driving the specular component Kajiya and Kay pointed out that reflection of a parallel beam from the surface of a cylinder will be in a cone centered on the hair axis whose angle of apex is equal to the incident angle (Refer to Appendix A). They conclude that the reflection from a non-ideal fiber should be a lobe centered on that cone. Because of this property, they introduced an ad hoc specular model which is similar in sprit to the specular highlight component of Phong shading model. They defined the specular reflection component as:

$$\Psi^{K\&K}_{Specular} = k_s \cos^p(\theta_r + \theta_i) \tag{11}$$

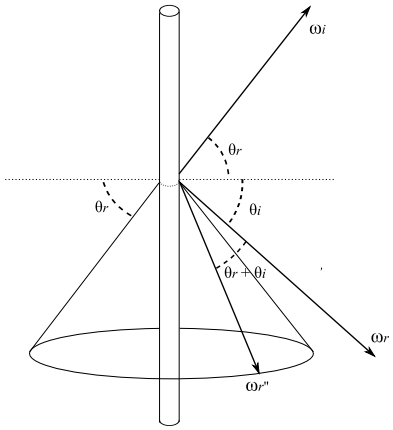

Figure 12: *Derivation of Kajiya and Kay's specular component.*

and the whole shading model is the sum of the diffuse and specular components:

$$\Psi^{K\&K} = \Psi^{K\&K}_{Diffuse} + \Psi^{K\&K}_{Specular} \tag{12}$$

In terms of the curve scattering function, we can express Kajiya and Kay's model as:

$$f_s^{K\&K}(\theta_i, \phi_i, \theta_r, \phi_r) = K_d + k_s \frac{\cos^p(\theta_r + \theta_i)}{\cos\theta_i} \tag{13}$$

And in terms of azimuthal and longitudinal scattering functions, we can express Kajiya and Kay's shading model as the following:

$$\begin{aligned}
f_s^{K\&K}(\theta_i, \phi_i, \theta_r, \phi_r) &= M^{K\&K}(\theta_i, \theta_r) \times N^{K\&K}(\phi_i, \phi_r) \\
M^{K\&K}(\theta_i, \theta_r) &= K_d + k_s \frac{\cos^p(\theta_r + \theta_i)}{\cos(\theta_i)} \qquad (14) \\
N^{K\&K}(\phi_i, \phi_r) &= 1 \qquad (15)
\end{aligned}$$

The model of Kajiya and Kay only has a longitudinal function and neither the peak value nor the width of the specular highlight is dependent on the azimuthal angles, ϕ_i or ϕ_r. It puts a constant intensity highlight lobe centered by the mirror reflection cone. For

the sake of comparison, we define the azimuthal scattering function for the model of Kajiya and Kay and set it to 1, which indicated that their model is not sensitive to the relative azimuthal angle.

With this simple model, Kajiya and Kay rendered furry objects using a novel three dimensional texture which they called *texels*. A texel is a 3D texture map which contains both the surface frame and lighting model parameters. Figure 13 shows one of their rendering results which was produced using their shading model. However, the specular highlight, which is the main feature of their shading model, is not significantly visible in their rendered images. Figure 14 shows our rendering results using the shading model of Kajiya and Kay. The main feature of their model which is the anisotropic primary highlight has been demonstrated in these images.

Figure 13: *Rendered teddy bear using the three dimensional textures and Kajiya and Kay's shading model. From [Kajiya and Kay 1989].*

5.2 Goldman 1997

In 1997, Goldman developed a number of refinements to the classical Kajiya and Kay's model in order to render furry animals in the movie industry. His main contribution in his paper was introducing an azimuthal dependence component for the hair scattering model. This refinement was based on the observation that hair behaves extremely different when it is lit from the front versus from the back side. Human hair fibers show a strong and highly directional forward scattering when they are lit from backside.

He introduced a relative directionality parameter κ for a given incident light ray ω_i, eye ray ω_r, and hair tangent direction $\vec{u}$ using the cosine of the dihedral angle between the planes containing each pair. In our notation, this can be expressed simply as $\kappa = \cos\phi$. Note that when ω_i and ω_r intersect with the hair from the same side (i.e in front-lighting), $\kappa > 0$, and when ω_i and ω_r point to the opposite sides of the hair (i.e in back-lighting), $\kappa < 0$.

He also defined two extra parameters, ρ_R and ρ_T, to control the amounts of forward and backward scattering properties of the hair fibers. Then he multiplied both terms of the Kajiya and Kay's model by an azimuthal scattering function, $N^{Goldman}$, which can be expressed as:

$$N^{Goldman}(\phi) = \frac{1+\kappa}{2}\rho_R + \frac{1-\kappa}{2}\rho_T \qquad (16)$$

In his original paper, he called this azimuthal scattering function

Figure 14: *Our rendered images using Kajiya and Kay's shading model. The primary highlight which is the main feature of this shading model is visible in the rendered images.*

f_{dir}, meaning that this function handles the directionality of the shading model. This extra coefficient, κ, controls the relative amount of forward transmission and backward reflection and adds azimuthal dependency to the Kajiya and Kay model. When $\kappa = 1$, the model returns Kajiya and Kay's shading result multiplied by ρ_R. When $\kappa = -1$, it returns the result of Kajiya and Kay's model multiplied by ρ_T. All other possible values for κ result in a weighted average of these two situations. Using this directional attenuation factor, Goldman was able to simulate the translucency of hair fibers. Parameters ρ_R and ρ_T are empirically set. Nearly equal coefficients would be used for white or gray hairs. Higher ρ_R results in simulating more pigmented hair and higher ρ_T simulates more translucent hair [Goldman 1997]. Note that setting ρ_R and ρ_T equal to one will result in the Kajiya and Kay model.

$$f_s^{Goldman} = f_s^{K\&K} \times N^{Goldman}(\phi) \qquad (17)$$

$$= M^{K\&K} \times N^{Goldman}(\phi) \qquad (18)$$

Goldman's emphasis was on rendering visual characteristics of fur in cases where the hair geometry is not visible at the final image resolution and where the hairs are relatively small so that the skin is partially visible. His second main contribution in his paper

Figure 15: *A frame from the film 101 Dalmatians. ©Disney 1996. Only the two adult dalmatians are photographs and all of the puppies in the scene are rendered using Goldman's shading model. From [Goldman 1997]*

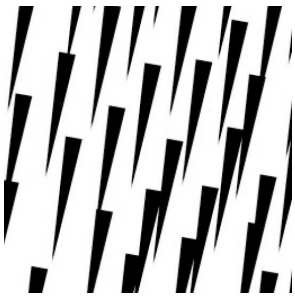

Figure 16: *Poisson disk distribution of triangles converted into a 2D texture. The goal of opacity function α_f is to predict the ratio of area covered by hair geometries to the overall area of the viewing image. From [Goldman 1997].*

[1997] was introducing the *fakefur opacity function* α_f. This function computes the mean opacity of a patch of fur as viewed from a given angle. Therefore, α_f is a function of the hair geometry, the distribution of hairs on the skin, and the viewing angle, ω_r.

For simplifying his calculations, Goldman assumed that all the hairs have similar shapes; long truncated cones with different radii at their base and tip, and that their projection into the viewing plane can be approximated by similar trapezoids. He also simplified the calculations by assuming that the distribution of hairs in a small region on the skin has Poisson characteristics (see Figure 17). He analytically calculated the expectation of a ray hitting a hair geometry from a given viewing angle and he introduced a probabilistic rendering algorithm which enabled him to blend the reflected light from hair fibers with the reflected light from the skin below the hairs. Goldman's fakefur opacity function is defined as:

$$\lim_{n_i \to \infty} \alpha_f = 1 - e^{-DA_h \cos\theta_i / \cos\xi} \tag{19}$$

where n_i is a constant denoting the number of hairs in the sampled region, D is the local density of hairs, A_h is the projected area of a single hair into the viewing plane and ξ is the angle between hair direction, $\vec{u}$, and skin surface normal. Figure 15 shows a frame of

Figure 17: *Our rendering result for a gray hair using Goldman's shading model.*

the movie *101 Dalmatians* where Goldman employed his shading model and his fakefur opacity function to render the furry dalmatians photorealistically. Figure 17 shows our rendering results for a gray colored hair using Goldman's shading model.

5.3 Kim 2002

Kim extended previous shading models in his PhD thesis by proposing a new set of azimuthal scattering functions which he referred to them as phase functions [Kim 2002]. Similar to Goldman's model, Kim's shading model is inspired by the observation that the scattering patterns of a hair fiber is significantly dependent on the relative azimuthal angle between the light source and the observer. (The

difference between front and back lighting).

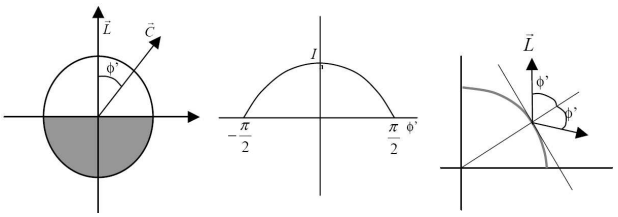

Figure 18: *Kim's demonstration for calculating the reflected component N_R^{Kim}. (left) The white region is illuminated by light from direction $\vec{L}$ (center) Lambertian illumination as a function of φ'. (right) Perfect mirror reflection of incident ray will have angle $2\varphi'$. From [Kim 2002].*

Kim's phase function consists of two terms: a reflection lobe, N_R^{Kim}, and a transmission lobe, N_T^{Kim}. The surface reflection lobe has been derived from the assumption of mirror reflection off a smooth Lambertian cylinder with no consideration for Fresnel term. For deriving this component, he considered the cross section of a cylinder by its normal plane (see Figure 18 left). Assuming that the light direction, ω_i, is $\vec{L}$, then the amount of observed Lambertian illumination, I_o form an incident light I is given by (see Figure 18 center):

$$I_o(\phi') \;=\; I\cos(\phi')\,,\; \frac{\pi}{2} \le \phi' \le \frac{\pi}{2} \tag{20}$$

and it is 0 otherwise. Besides, the angle of reflected ray is always $2\phi'$ (see Figure 18 right) so the reflection phase function would be

$$N_R^{Kim}(\phi') \;=\; \cos(\frac{\phi'}{2})\,,\; -\pi \le \phi' \le \pi \tag{21}$$

The polar plot of the reflection phase function is like a upside-down heart (see Figure 22), which is obviously different from Kajiya and Kay constant azimuthal function. (see Section 7 for more discussion).

Kim observed that due to refraction, hair fibers show strong forward scattering behaviors. He approximated the forward scattering property with a single cosine lobe which he called the transmission lobe. His approximation for the transmission lobe is:

$$N_T^{Kim}(\phi') \;=\; \cos(\,k\,(\phi' - \pi))\,,\; |\phi'| \ge \pi(1 - \frac{1}{2k}) \tag{22}$$

and it is 0 otherwise. The parameter k controls the sharpness of the transmission component. The larger the k the sharper is the scattering lobe. At the end, he combines these two phase function together to have a single phase function in a similar manner to Goldman [1997]:

$$N^{Kim}(\phi) = \rho_R N_R^{Kim}(\phi) \;+\; \rho_T N_T^{Kim}(\phi) \tag{23}$$

Kim shading model for hair would be the multiplication of N^{Kim} with the result of Kajiya and Kay shading model and we have:

$$f_s^{Kim} \;=\; f_s^{K\&K} \times N^{Kim}(\phi) \tag{24}$$

$$\;=\; M^{K\&K} \times N^{Kim}(\phi) \tag{25}$$

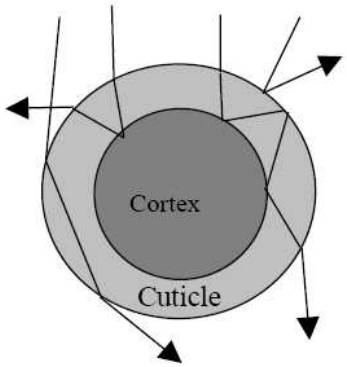

Figure 19: *Kim's Monte Carlo simulation model. From [Kim 2002].*

In order to verify his proposed phase function, Kim modeled hair fibers as a transparent cuticle layer covering an absorbent cortex layer and plotted its phase function by a Monte Carlo path-tracing simulation. In his simulation, he accounted for the Fresnel term and multiple scattering of light inside the hair fiber (see Figure 19). He showed that his simplified phase functions can cover a large range of similar phase functions to his Monte Carlo simulation. He mentioned in his observations from his Monte Carlo simulation that "two small peaks can be observed diagonally in the reflection phase" [Kim 2002], but he did not try to model them or verify their sources. These peaks are the internal caustics and are result of light reflections from inside of the fiber. Later, these internal caustics were called glints by Marschner et al. [2003].

Figure 20: *Kim's rendering result. (left) Rendered image using Kim's shading model. (right) Comparison with a photograph. From [Kim 2002].*

Kim's model is similar to the model of Goldman [1997]. However, the plot of the azimuthal function of Goldman's model is very limited and the ability to change the sharpness of the transmission component term is missing. Refer to Section 7 for more discussion and comparisons. Figure 20 shows a comparison between a rendered image using Kim's shading model and a photograph. You can see our rendered images which have used Kim's shading model in Figure 21.

5.4 Marschner 2003

Marschner et al. extended previous models and introduced a physically based scattering model for rendering hair fibers [Marschner et al. 2003] which has remained to be the basis of all modern shading models in the field of rendering fibers. Beside their novel shading model, they have reported the most comprehensive light scattering measurements which we have discussed in Section 3.

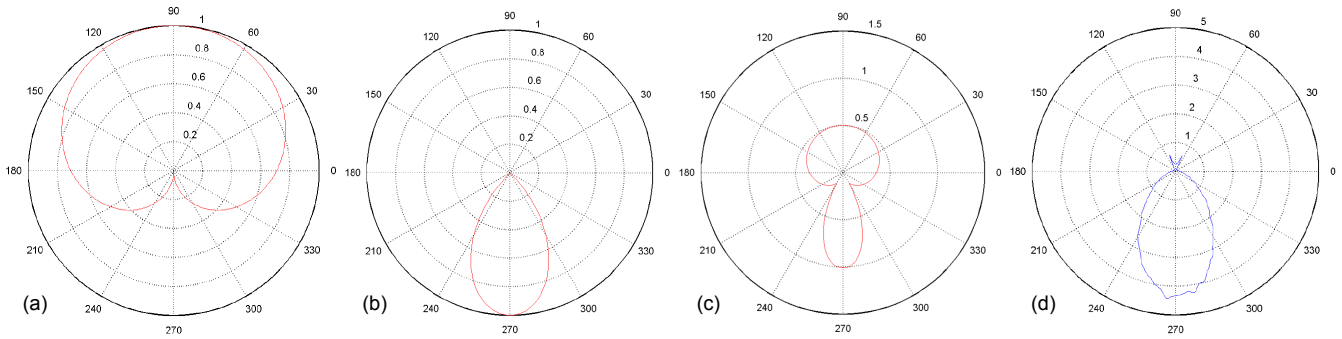

Figure 22: *Kim's azimuthal scattering function components. (a) Reflected component N_R^{Kim}.(b) Transmitted component N_T^{Kim} with $k = 2.0$. (c) Combined azimuthal scattering function N^{Kim} with $\rho_R = 0.5$, $\rho_T = 1.0$, and $k = 3.0$. (d) Kim's Monte-carlo path-tracing simulation for $\eta = 1.5$ and his observation of the diagonal glints. From [Kim 2002].*

Figure 21: *Our rendering results using Kim's shading model. The forward scattering component has been improved substantially from the previous shading models.*

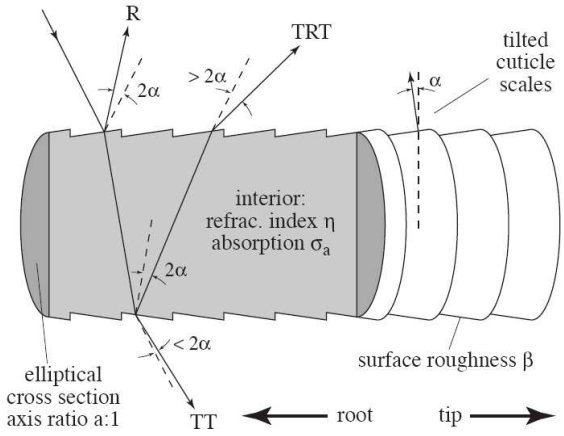

Figure 23: *A schematic of the model of Marschner et al. for simulating the light scattering by hair fibers. Dashed lines show the direction of scattering angles in the absence of tilted cuticle scales. From [Marschner et al. 2003].*

Their contributions include substantial improvements on both longitudinal and azimuthal scattering functions. They considered the separation of surface reflection highlight (R), transmitted component (TT) and internal-reflection component (TRT). They have also provided analytical analysis for predicting azimuthal variation based on the ray optics of smooth cylinders.

Their model is the first to improve the longitudinal scattering functions by including the effect of tilted cuticles. As previously mentioned, the cuticles are tilted toward the root of the hair (approximately by 5^o) and they shift the reflection cones of the primary and secondary highlight (internally reflected highlight) slightly off the ideal mirror reflection cone. Considering this effect may sound trivial but these tilted cuticles produce a very significant visual effect, which is the separation of primary and secondary highlight. As illustrated in Figure 23, this slight shift in normal direction will result in shifts in opposite direction for R and TRT components which causes the separation of these two highlights. Primary highlight is always shifted toward the root of the hair, whereas secondary highlight is shifted toward the tip of the hair. Therefor primary highlight always appears below the secondary highlight.

Their improvements on azimuthal scattering functions include the analytical analysis for predicting the intensity of reflected light based on the ray optics of a circular cross section, considering the Fresnel term when light interacts with the boundary of the fiber, and accounting the volume absorption of internal medium.

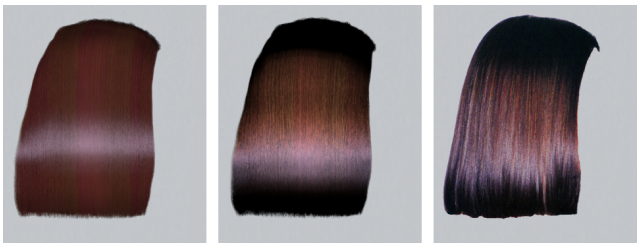

Figure 24: *Comparison between (left) Kajiya and Kay's model, (center) model of Marschner et al., and (right) a photograph. From [Marschner et al. 2003].*

Their final scattering model consists of three longitudinal functions, M, and three azimuthal functions, N, for each scattering mode: reflected component by fiber's surface, transmitted component throw the fiber and reflected light form inner surface of the fiber.

$$\begin{aligned} & f_s^{Marschner}(\phi_i, \theta_i; \phi_r, \theta_r) = \\ & M_R^{Marschner}(\theta_h, \theta_d)\, N_R^{Marschner}(\phi, \eta') + \\ & M_{TT}^{Marschner}(\theta_h, \theta_d)\, N_{TT}^{Marschner}(\phi, \eta') + \\ & M_{TRT}^{Marschner}(\theta_h, \theta_d)\, N_{TRT}^{Marschner}(\phi, \eta^\star). \end{aligned} \tag{26}$$

In this equation, longitudinal functions (M) are normalized Gaussian divided by $\cos^2\theta_d$, where the $\cos^2\theta_d$ term accounts for the projected solid angle. Each Gaussian lobe is centered around its corresponding shifted reflection cone. (The shift is different for each scattering mode and are set by the user with α_R, α_{TT}, and α_{TRT} parameters) with user-defined standard deviations β_R,β_{TT} and β_{TRT}. Mathematical equations for the longitudinal scattering functions are listed here:[2]

$$M_R^{Marschner}(\theta_h, \theta_d) = g(\beta_R, \theta_h - \alpha_R)/\cos^2\theta_d \tag{27}$$

$$M_{TT}^{Marschner}(\theta_h, \theta_d) = g(\beta_{TT}, \theta_h - \alpha_{TT})/\cos^2\theta_d \tag{28}$$

$$M_{TRT}^{Marschner}(\theta_h, \theta_d) = g(\beta_{TRT}, \theta_h - \alpha_{TRT})/\cos^2\theta_d \tag{29}$$

Azimuthal functions N take into account the Fresnel terms, internal absorption terms and ray-density factors.

$$N_R^{Marschner} = A_R |2\frac{d\phi}{dh}(\phi)|^{-1} \tag{30}$$

$$N_{TT}^{Marschner} = A_{TT} |2\frac{d\phi}{dh}(\phi)|^{-1} \tag{31}$$

$$N_{TRT}^{Marschner} = \sum_{root=0}^{roots} A_{TRT} |2\frac{d\phi}{dh}(\phi)|^{-1} \tag{32}$$

where $roots$ is either 1 or 3 and indicates that potentially three different azimuthal offsets of incident light can result in the same relative azimuthal angle, ϕ. Attenuation factors, A_R, A_{TT} and A_{TRT}, combine the Fresnel attenuation factor with internal absorption term and we have:

$$A_R = F(\eta', \eta'', \gamma_i) \tag{33}$$

$$A_{TT} = (1 - A_R)^2\, e^{-\sigma_a l} \tag{34}$$

$$A_{TRT} = A_{TT}\, F(1/\eta', 1/\eta'', \gamma_t)\, e^{-\sigma_a l} \tag{35}$$

where l is the length of the path inside the fiber which is mistakenly stated to be $2 + 2\cos\gamma_t$ but it is in fact square root of the mentioned value and is equal to $2\cos(\gamma_t)$.

Since the shading model of Marschner et al. [2003] is based on analytical solution for perfect smooth cylinders, caustics in their TRT component produces singularities with infinite intensity in $f_s^{Marschner}$. In the real world, these caustics will be smoothed out because of surface roughness. Marschner et al. addressed this issue by removing the caustics from TRT and replacing them with Gaussian lobes. This non-physically based way of handling glints is one of the main drawbacks of their model especially because user can make the replaced Gaussian lobes arbitrary large and wide.

[2] Marschner et al. [2003] considered the term $1/\cos\theta_d^2$ outside of the longitudinal and azimuthal scattering functions.

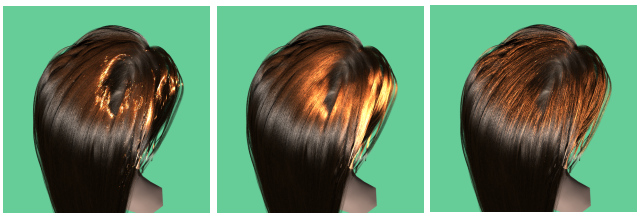

Figure 25: *Our visualization of the proposed method for fixing the singularities in the azimuthal scattering function by Marschner et al. (left) Rendering result by assuming that hairs are perfect smooth cylinders. (center) Replacing the sharp peaks with smooth Gaussian lobes. (right) Simulating different eccentricities with adjusting the index of refraction for each hair.*

As we mentioned in Section 3, hair fibers are usually elliptical, rather than circular. In this case, there is no simple analytical solution for the azimuthal scattering functions. The component which is affected by eccentricity the most is the TRT component. The caustic's angle of appearance changes drastically by a slight change in eccentricity. Marschner et al. state that "Changing refractive index has effects that are qualitatively similar to changing eccentricity." As a result, they approximate the effect of eccentricity by changing the index of refraction to $\eta^\star$ for calculation related to TRT component. They show that a reasonable choice for $\eta^\star$ is:

$$\begin{aligned} \eta_1^\star &= 2(\eta - 1)a^2 - \eta + 2 \\ \eta_2^\star &= 2(\eta - 1)/a^2 - \eta + 2 \\ \eta^\star(\phi_h) &= \frac{1}{2}((\eta_1^\star + \eta_2^\star) + \cos(2\phi_h)(\eta_1^\star - \eta_2^\star)) \end{aligned} \tag{36}$$

where a is the eccentricity of the fiber ($a = 1$ for circular cross sections). Having random eccentricity values for individual hair fibers causes the glints to appear in random azimuthal angles and therefore gives texture to the assembly of hair strands. Figure 25 shows different steps in handling the glints in model of Marschner et al. [2003] including the effect of simulating random eccentricity.

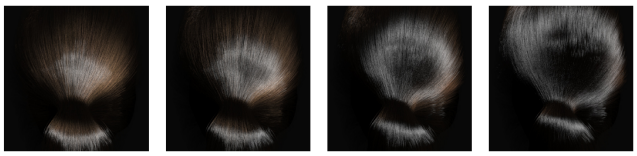

Figure 26: *A hair model under different illumination angles rendered by the model of Marschner et al. From [Marschner et al. 2003].*

5.5 Zinke 2004, 2007

Zinke extended Marschner's model in two publications [Zinke et al. 2004; Zinke and Weber 2007] and also in his PhD thesis [Zinke 2007], which made it more suitable for simulating multiple scattering. He generalized the previously developed model of Marschner et al. [2003] by taking into account the longitudinal movement of

Figure 27: *Our rendering results using the model of Marschner et al. Presence of secondary highlight adds a lot to the realism of the rendered images.*

light inside the fiber and also azimuthal offset of the incident and scattered light. The shading model of Marschner et al. assumes that the viewer and light source are far away from the assembly of hair fibers and so it ignores the microscopic azimuthal and longitudinal offsets. However, these *far-field* lighting and viewing assumptions are not obviously true in the case of indirect illumination. Multiple scattering of light among hair strands should be modeled more accurately by accounting for the microscopic azimuthal and longitudinal offsets. Zinke referred to his generalized shading model as a *near-field* scattering model. If we consider the azimuthal offset of the incident beam and refracted beam to be h_i and h_r, respectively, and the longitudinal offset to be Δs, then Zinke's shading model can be expressed as:

$$\begin{aligned} f_s^{Zinke}(\phi_i,\theta_i,h_i;\phi_r,\theta_r,h_r;\Delta s) \quad = \\ M_R^{Zinke}(\theta_h,\theta_d,\Delta s)\, N_R^{Zinke}(\phi,\eta',h_i,h_r) + \\ M_{TT}^{Zinke}(\theta_h,\theta_d,\Delta s)\, N_{TT}^{Zinke}(\phi,\eta',h_i,h_r) + \\ M_{TRT}^{Zinke}(\theta_h,\theta_d,\Delta s)\, N_{TRT}^{Zinke}(\phi,\eta^\star,h_i,h_r) \end{aligned} \tag{37}$$

where his longitudinal scattering functions are defined as:

$$M_R^{Zinke}(\theta_h,\theta_d,\Delta s) = M_R^{Marschner}(\theta_h,\theta_d) \times \delta(\Delta s) \tag{38}$$

$$M_{TT}^{Zinke}(\theta_h,\theta_d,\Delta s) = M_{TT}^{Marschner}(\theta_h,\theta_d) \times \delta(\Delta s + s_{TT}) \tag{39}$$

$$M_{TRT}^{Zinke}(\theta_h,\theta_d,\Delta s) = M_{TRT}^{Marschner}(\theta_h,\theta_d) \times \delta(\Delta s + s_{TRT}) \tag{40}$$

which means that we can measure the intensity only where the difference in longitudinal offsets are equal to the exact distance that light moves inside the fiber. For reflection, this azimuthal difference is zero and for TT and TRT component the following formula yields the displacement distances.

$$s_{TT} = l\tan\theta_t \tag{41}$$

$$s_{TRT} = 2l\tan\theta_t \tag{42}$$

Zinke's azimuthal scattering functions are again based on Marschner's azimuthal scattering functions and are defined as:

$$N_R^{Zinke}(\phi,\eta') = N_R^{Marschner}(\phi,\eta') \times \delta(h_i + h_r) \tag{43}$$

$$N_{TT}^{Zinke}(\phi,\eta') = N_{TT}^{Marschner}(\phi,\eta') \times \delta(h_i + h_r) \tag{44}$$

$$N_{TRT}^{Zinke}(\phi,\eta^\star) = N_{TRT}^{Marschner}(\phi,\eta^\star) \times \delta(h_i + h_r) \tag{45}$$

Figure 28: *Rendering blond hair with multiple scattering. (Left) Direct illumination with the model of Marschner et al. (Right) Multiple scattering with Zinke's shading model. From [Zinke et al. 2004].*

which means that the intensity can be measured only if $h_i = -h_r$. Authors replaced delta functions with normalized Gaussian lobes to take into account surface roughness. We will see in Section 7 that these considerations are necessary even in the case of single scattering but they become more crucial in the case of simulating multiple scattering. With these two extensions to Marschner model, Zinke could simulate multiple scattering of light inside the hair volume, which is important for rendering blond hair, more accurately. Figure 28 shows rendering of a blond hair using Zinke's shading model compared to Marschner's shading model [Zinke et al. 2004]. However, the comparison is not fair since it is comparing Marschner's model with single scattering with Zinke's model with multiple scattering. Figure 29 shows our comparison between Zinke's model and Marschner's model both with multiple scattering. For a through comparisons between these two shading models refer to Section 7.

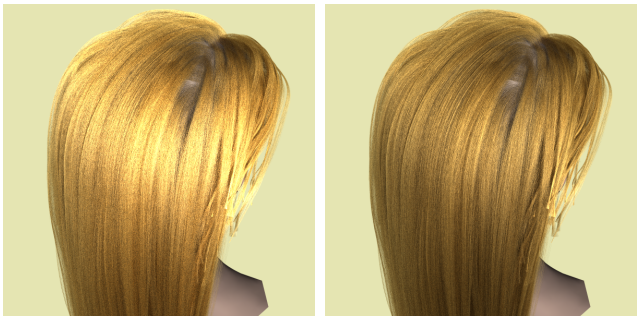

Figure 29: *Our comparison between the result of (left) the model of Marschner et al. with multiple scattering, and (right) Zinke's shading model with multiple scattering.*

6 Multiple Scattering in Hair Rendering

Multiple scattering plays a significant role in hair rendering, especially in the case of rendering blond hair. Considering the effect of shadowing and attenuation alone is not sufficient for producing the correct appearance of human hair. In this section, we briefly mention prominent works in literature that have tackled the problem of simulating multiple scattering of light inside hair volume. We separate the works in this category into three main subsections: path-tracing approaches, photon-mapping approaches, and approximation approaches. In the rest of this section we will briefly discuss the main works in each subcategory.

Figure 30: *Rendering an assembly of blond hairs with Zinke's shading model and increasing the depth of scattering from 1 (left) to 4 (right). From [Zinke et al. 2004].*

There have been some attempts to simulate multiple scattering in hair rendering by using Monte Carlo path-tracing mainly by Zinke et al. [Zinke et al. 2004; Zinke and Weber 2007; Zinke 2007]. We have already discussed the generalizations that Zinke has made to the model of Marschner et al. He considered the effect of microscale azimuthal and longitudinal offsets in the model of Marschner et al. Theses considerations are important especially in the case of simulating multiple scattering. Figure 28 shows a comparison between single scattering (Marschner model) and multiple scattering (Zinke model) for rendering blond hair. For a more thorough comparison, refer to Section 7. Extending the single scattering shading model to a Monte Carlo path-tracing shading model that accounts for multiple scattering is straightforward and can be done without much modification to the shading model. Zinke showed in his [2004] paper that for blond hairs, the effects of indirect illumination and multiple scattering inside hair volume can result in visible differences up to a scattering depth of about five (see Figure 30). However, this depth can become arbitrary large by reducing the absorbtion coefficient of the hair fibers.

Figure 31: *Rendering results of a ponytail lit from the front. (left) Single scattering result. (center) Path tracing results after 60 hours (right) Moon and Marschner's photon map based approach in 2.5 hours. From [Moon and Marschner 2006].*

Conventional path-tracing approaches are computationally very expensive and their rendering result converges very slowly. There have been two concurrent works by [Moon and Marschner 2006] and [Zinke and Weber 2006] which try to simulate the effect of multiple scattering in hair rendering based on photon mapping [Jensen 2001]. Both methods extend the conventional photon mapping algorithm to make it more suitable for the complex optical and geometrical properties of hair fibers. Moon and Marschner [2006] store their photons in a 5D position-direction data structure to allow for the very directional radiance distributions that are present in hair volume. Also, they store photons along the paths rather than at the scattering points. Together with a novel radiance caching scheme, they capture the effect of multiple scattering in light-colored hair in 1 to 2 orders of magnitude faster than path tracing methods. Zinke and Weber [2006] base their method on the ray mapping approach [Havran et al. 2004], where they store not only the photons, but also the whole photon paths in the photon map. Havran et al. show that ray maps eliminate the boundary bias and reduce topological bias of density estimate in global illumination [2004]. Figure 31 shows the rendering results of [Moon and Marschner 2006] where they compare the results of their photon mapping method with a path traced image and a photograph. Zinke and Weber also have a comparison between the results of their method and a path tracing method. Both methods produce similar results to the path tracing approach in significantly lesser time (see Figure 32).

Figure 32: *Rendering results of an assembly of light colored hair strands. (left) Single scattering results. (center) Zinke and Weber photon mapping approach in 250 seconds. (right) Path tracing result after 22000 seconds. From [Zinke and Weber 2006]*

.

Recently there has been a work by Zinke et al. [2008] that approximates the indirect illumination inside the hair volume for fast simulation of multiple scattering. Their work is similar in spirit to the works in the field of participating media [Premoze et al. 2004] and rendering translucent materials [Chen et al. 2004]. They introduce the concept of dual scattering, which splits the multiple scattering component into *global multiple scattering* and *local multiple scattering* components. The global multiple scattering component is responsible for computing the irradiance arriving at the neighborhood of a point inside the hair volume and the local multiple scattering component approximates the multiple scattering of incoming irradiance within this local neighborhood. After numerous simplifications and pre-computations they are able to render images similar to the results of path tracing method but in orders of magnitude less time. They also have a GPU-based implementation that produces similar results in real time (see Figure 33 for a comparison).

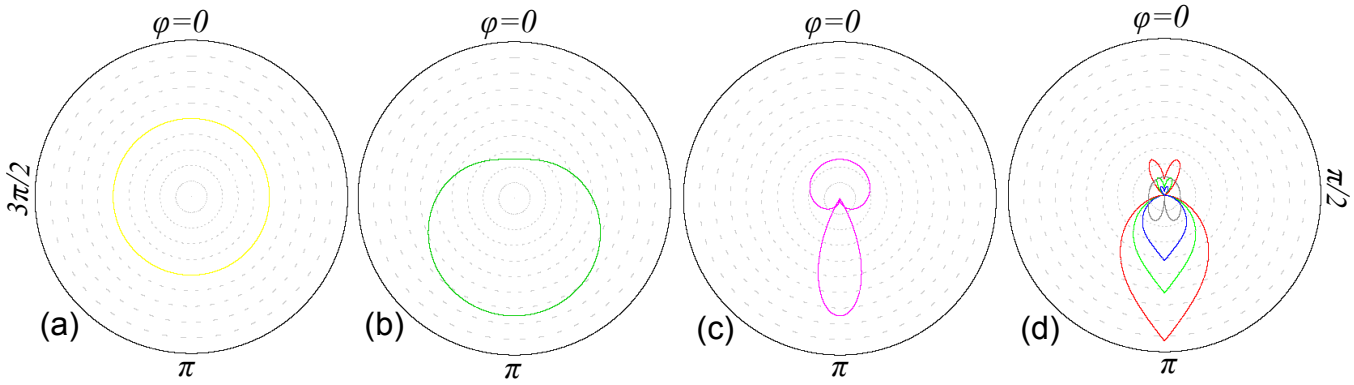

Figure 34: *Evolution of Azimuthal scattering functions: (a) shows the azimuthal independent model of Kajiya and Kay, (b) shows the effect of Goldman's refinements to the Kajiya and Kay's model. (c) shows the combined phase function of Kim model with the upper lobe being the reflected component and the lower sharper lobe being the transmitted component, and (d) plots the physically based model of Marschner et al. The gray plot which resembles a flipped heart is the R component, the colored lower lobes present the TT component, and three colored upper lobes which look like hearts represent the TRT component (glints), Zinke has used the azimuthal scattering function of Marschner et al.*

Figure 33: *Dual scattering approximation results. (left) Path tracing result after 7.8 hours. (center) Dual scattering method in 5.2 minutes. (right) GPU based dual scattering method in real-time with 14fps. From [Zinke et al. 2008].*

7 Summary and Comparison

In this section, we summarize all the discussed shading models, show how these models have been built up on top of each other, and how they have evolved over the years. In the remaining of this section we will discuss the strengths and weaknesses of each model and emphasize their main contributions. In addition, we have implemented all of the discussed shading models and will compare their rendering results with each other.

7.1 Evolution of Shading Models

The shading model of Kajiya and Kay [1989] is the ancestor of all modern hair rendering models. Kajiya and Kay introduced the geometrical properties of reflections of a parallel beam of light off a cylindrical surface. In other words, their main contribution is introducing the longitudinal scattering function for a smooth cylinder to the graphics community. However, their model puts a constant intensity highlight all around the hair fiber and it is not sensitive to the relative azimuthal angle. Also, their shading model models the hair fibers as opaque cylinders and so it only takes into account the single reflection, R, off the outer surface of the fiber. It does not take into account the strong forward scattering component (TT) and all other scattering modes like secondary highlight (TRT) and multiple scattering component have been simulated using a diffuse term that produces radiance proportional to the cosine of the incident angle. Their calculations for computing the diffuse component is not accurate since it does not consider the visibility term and it assumes that all the lit surface of the hair is visible to the viewer. In general, Kajiya and Kay's model is not physically based and not energy conservative. Kajiya and Kay's model is able to approximately capture the behavior of dark hair where only the R component is important.

Goldman built his shading model on top of Kajiya and Kay's model by extending it to account for transmission component [Goldman 1997]. His main contribution would be separating the reflected component from the transmission component. His model is sensitive to the relative azimuthal angle. However, his introduced parameters are purely empirical and arbitrary. His generalizations have no physically based basis and his model suffers from all mentioned limitations for the model of Kajiya and Kay. One main problem with his model is that the backward reflection component merges into the strong forward scattering component smoothly which does not match the empirical measurements (See Figure 34). We will discuss this issue later in the text in Section 7.

Kim extended Goldman's model in his PhD thesis [Kim 2002] and improved the reflection component, R, and made it more physically based. Actually his R component is completely physically based except he did not consider Fresnel attenuation factors in his calculations. He also improved Goldman's transmission component substantially by replacing it with a single cosine lobe. His transmission component could match his Monte Carlo simulated behavior of the light scattering of a fiber more closely than Goldman's model. However, his transmission lobe is still empirical and the parameters for controlling it were arbitrary. Kim also observed glints in his Monte Carlo simulation but he did not simulate them or investigate their origin.

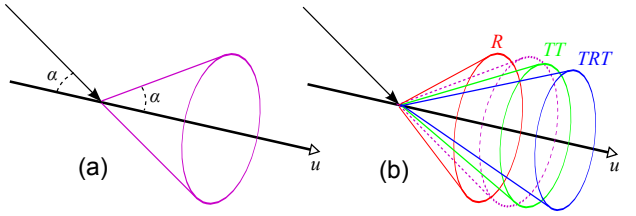

Figure 35: *Evolution of longitudinal functions: (a) Before the model of Marschner et al. (Kajiya and Kay, Goldman and Kim) (b) After the model of Marschner et al. (Marschner et al. and Zinke)*

Marschner et al. [2003] made huge contributions in the field of hair

rendering and presented a sophisticated physically based light scattering model. They introduced the longitudinal separation of the highlights into surface reflection (R), forward transmission (TT), and internal-reflection component (TRT) due to tilted cuticle angles. They also predict the azimuthal behavior of each light scattering component based on the ray optics of a circular cross section cylinder. Their derived reflection component, R, is basically Kim's reflection lobe multiplied with the Fresnel term. In contrast, their TT component is physically based and takes into account the Fresnel term and absorption of light in the interior of the fiber. They introduced secondary highlight component, TRT, along with its separation from the R component for the first time to the graphics community. They also observed and simulated the internal caustics (glints) that form inside the cylinder and they approximated the effect of eccentricity for circular hair fibers.

Despite the great contributions and strong physical basis of the model presented in [Marschner et al. 2003], Marschner's model exploits a lot of non-physically based approximations. For example, they used empirical Gaussian lobes for simulating the roughness of the surfaces and for smoothing out the caustics for handling the glints. Also, their TRT term is not energy conservative since one can scale the Gaussian lobes used for smoothing out the glints to become arbitrary wide and tall.

There is an additional flaw in the shading model of Marschner et al. [2003]. This model calculates the maximum illumination that can be perceived for different scattering components, adds them together, and returns this maximum value as the final radiance. This means that the shading model of Marschner et al. will always return the maximum value for radiance over the whole cross section of the hair fiber. This will result in minor visual differences in simulating single scattering for hair fibers which are very small in the image plane. However, when the viewer and light are not far from the hair strands, this inaccuracy causes more problems and so for simulating multiple scattering, more accurate calculations are needed.

Zinke et al. address the problem mentioned in last paragraph about the model of Marschner et al. [2003]. Zinke et al. adjust the model of Marschner et al. in order to simulate multiple scattering [Zinke et al. 2004; Zinke and Weber 2007] by accounting for the azimuthal and longitudinal offsets. In fact the effect of azimuthal offsets is very crucial for guaranteeing the energy conservation by the model of Marschner et al. but longitudinal offsets are only important for the close-up scenes and can be ignored in the case of far field viewing. However, Zinke's shading model suffers form the other problems that have been mentioned for the model of Marschner et al. We have to point out that the comparisons in Zinke's publications are between Marschner's shading model with single scattering with Zinke's shading model with multiple scattering (Figure 28). In Section 7.3 we provide a more comprehensive comparison between these two models both in the case of single scattering and multiple scattering.

7.2 Evolution of Longitudinal and Azimuthal Scattering Functions

Here we investigate the development of longitudinal and azimuthal scattering functions one by one. Longitudinal scattering functions are the ones who dominate the final visual appearance of the shading model (see Figure 37) and so they play a very important role in all shading models. However, there has not been many changes to the longitudinal scattering function over the years. The model of Kajiya and Kay [1989] is solely a longitudinal scattering function. Goldman [1997] and Kim [2002] use the same longitudinal scattering function in their models. Marschner et al. [2003] consider the effect of tilted cuticle angles and introduce three different

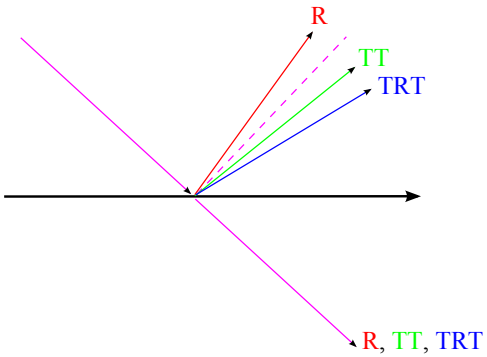

Figure 36: *Corrected model for simulating the reflection from a cone. Reflections from the front-lighting will be affected by the tilted cuticle angles whereas the reflections form back-lighting will be along the mirror reflection direction.*

directions for different light scattering components, which is basically three cones with different apex angles. (see Figure 35). Zinke et al. use the same longitudinal function as the one introduced by Marschner et al. [2003].

It is worthwhile to point out that none of these longitudinal scattering functions are actually correct. The correct longitudinal function would be the reflection of a parallel incident beam off a cone (due to tilted cuticle angles), which is more complicated than just a simple cone. As shown in Figure 36, in the case of front-lighting, different components will reflect with diffract angles; but in the case of back-lighting, all component would overlap. One can approximate the result by averaging between these two extremes but the exact solution is more complicated than this approach.

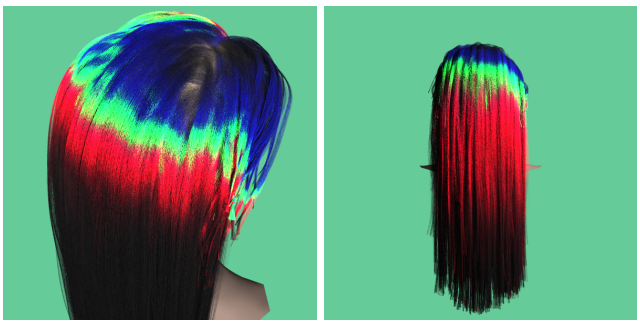

Figure 37: *Longitudinal functions dominate the final appearance of the shading model by separating the highlights. Red, Green, and Blue colors visualize R, TT, and TRT component.*

Azimuthal scattering functions have undergone more changes during the years. They started from a simple constant azimuthal scattering function of Kajiya and Kay [1989] to a very sophisticated triple azimuthal function of Marschner et al. [2003] (see Figure 34 for a visual demonstration of these changes). Model of Kajiya and Kay [1989] is not sensitive to relative azimuthal angle ϕ. Goldman [1997] adds a little bit of azimuthal sensitivity to the model of Kajiya and Kay and Kim [2002] extends this model to have two separate lobes for reflection and transmission component. Marschner et al. [2003] developed a sophisticated triple of azimuthal function, which has been used in later models [Zinke et al. 2004; Zinke and Weber 2007].

Figure 38: *Our comparison between different shading models for rendering dark hair. Top row demonstrates the forward scattering effect and bottom row shows the result of primary (and secondary) highlight(s). A dark brown color has used as a diffuse component for the model of Kajiya and Kay, Goldman, and Kim. For the model of Marschner et al. no diffuse color has been used and all the coloration is due to absorption.*

7.3 Rendering Results

We have implemented all discussed light scattering models including the classical model of Kajiya and Kay [1989], Goldman's model [1997] , Kim's model [2002], sophisticated model of Marschner et al. [2003], and Zinke's shading model [Zinke et al. 2004; Zinke and Weber 2007]. All the images have been rendered by the author's personal global illumination renderer, *Mirage*. Here, we present rendered images by employing different shading models and compare them with each other.

Figure 38 shows the comparison between the rendering results of models of Kajiya and Kay, Goldman, Kim, and Marschner. These models are appropriate for rendering dark hair. Top row demonstrates the ability of the model in handling the forward scattering of light. The bottom row shows how these models simulate the backward scattering components (primary and secondary highlights). Figure 39 illustrates our comparison between the model of Marschner et al. and Zinke's shading model for rendering blond hair. We have compared these two models in the case of single scattering (direct illumination), indirect illumination, and different depths of simulating the multiple scattering component. The difference is more noticeable in higher recursion depths for simulating the multiple scattering.

8 Missing Behaviors and Future Works

In this section, we point out the empirical measurements which are missing in the behavior of current shading models. As we mentioned in Section 3, there is a true specular highlight which appears on the exact mirror reflection at the grazing incident angles. This highlight is completely missing in the current modern shading models. In modern models we will always have the effect of tilted cuticle angles which will cause the reflection direction be away from mirror reflection direction.

Another important issue with current models are that they approximate the roughness of the surface of the hair fibers by empirical lobes (powers of cosine functions or normalized Gaussian lobes), and the analytical simulation of surface roughness is completely missing from the current models. Accounting for roughness will make the current shading models more robust and avoid using arbitrary heuristics in hair rendering, such as user-defined parameters to adjust the sharpness of the forward scattering components [Kim 2002], non-physically based way of handling glints [Marschner et al. 2003], etc. More accurate models for simulating the effect of roughness will probably help the prediction of the true specular reflection in the grazing angles.

One more avenue for improvement would be modeling the effect of eccentricity more accurately. Also, the current way of handling eccentricity by [Marschner et al. 2003] approximates the effect of eccentricity on the ray density factor but not on the Fresnel attenuation factor. This will effectively limits the qualitative accuracy of the proposed energy distribution function proposed by Marschner et al. [2003]

In addition, as we mentioned in Section 7, none of the proposed longitudinal scattering functions are actually correct. By considering the tilted cuticle angles, we cannot use the theory of reflections from a smooth cylinder. Analytical calculations for finding the exact longitudinal reflections from a smooth cone would solve this problem.

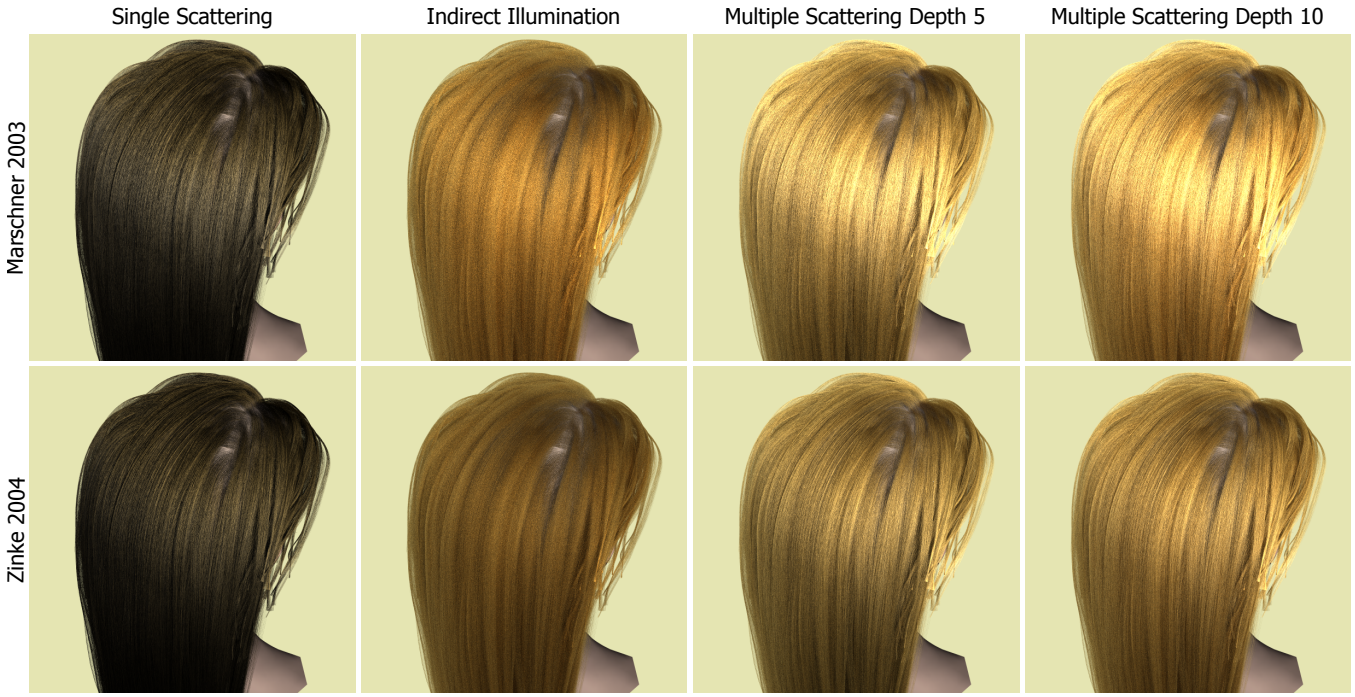

Figure 39: *Our comparison between the model of Marschner et al. and Zinke's generalized model. The effect of Zinke's generalizations becomes more visible by increasing the recursion depth for simulating the multiple scattering effect.*

9 Conclusion

In this paper we have presented a detailed overview over the most prominent hair shading models. We have also briefly looked over the physical properties of human hair fibers and attempts for simulating multiple scattering in hair rendering. We have implemented all of the discussed shading models and critically analyzed each shading model with emphasizing on their contributions, strengths, and weaknesses. Furthermore, we have mentioned missing behaviors in current shading models compared to the experimental measurements and proposed possible avenues for further research in the future.

Acknowledgements

I would like to thank Walt Disney Animation Studios for the hair model that has been used in our renderings. I would also like to thank my advisor Henrik Wann Jensen for related constructive discussions, Matthias Zwicker for pointing out the problem regarding to the reflections from a cone, Krystle de Mesa for proofreading a draft of this paper. This research was supported by a fellowship from Walt Disney Animation Studios.

References

ADLER, C. L., L. J. A., AND STONE, B. R. 1998. Rainbow scattering by a cylinder with a nearly elliptical cross section. *Applied Optics 37*, 15401550.

BANKS, D. C. 1994. Illumination in diverse codimensions. Tech. rep.

BUSTARD, H. K., AND SMITH, R. W. 1991. Investigation into the scattering of light by human hair. *Applied Optics*, 3485–3491.

CHEN, Y., TONG, X., WANG, J., LIN, S., GUO, B., AND SHUM, H.-Y. 2004. Shell texture functions. *ACM Trans. Graph. 23*, 3, 343–353.

GOLDMAN, D. B. 1997. Fake fur rendering. In *SIGGRAPH '97: Proceedings of the 24th annual conference on Computer graphics and interactive techniques*, ACM Press/Addison-Wesley Publishing Co., New York, NY, USA, 127–134.

HAVRAN, V., BITTNER, J., AND SEIDEL, H.-P. 2004. Ray maps for global illumination. In *SIGGRAPH '04: ACM SIGGRAPH 2004 Sketches*, ACM, New York, NY, USA, 77.

JENSEN, H. W. 2001. *Realistic image synthesis using photon mapping*. A. K. Peters, Ltd., Natick, MA, USA.

KAJIYA, J. T., AND KAY, T. L. 1989. Rendering fur with three dimensional textures. In *SIGGRAPH '89: Proceedings of the 16th annual conference on Computer graphics and interactive techniques*, ACM, New York, NY, USA, 271–280.

KIM, T.-Y. 2002. *Modeling, rendering and animating human hair*. PhD thesis, Los Angeles, CA, USA. Adviser-Ulrich Neumann.

LU, R., KOENDERINK, J. J., AND KAPPERS, A. M. L. 2000. Specularities on surfaces with tangential hairs or grooves. *Comput. Vis. Image Underst. 78*, 3, 320–335.

MARCUSE, D. 1974. Light scattering from elliptical fibers. *Applied Optics 13*, 19031905.

MARSCHNER, S. R., JENSEN, H. W., CAMMARANO, M., WORLEY, S., AND HANRAHAN, P. 2003. Light scattering from human hair fibers. In *SIGGRAPH '03: ACM SIGGRAPH 2003 Papers*, ACM, New York, NY, USA, 780–791.

MARSCHNER, S. 2005. Realistic materials in computer graphics: Scattering from fibers, course10,siggraph2005.

MOON, J. T., AND MARSCHNER, S. R. 2006. Simulating multiple scattering in hair using a photon mapping approach. In *SIGGRAPH '06: ACM SIGGRAPH 2006 Papers*, ACM, New York, NY, USA, 1067–1074.

MOON, J. T., WALTER, B., AND MARSCHNER, S. 2008. Efficient multiple scattering in hair using spherical harmonics. *ACM Trans. Graph. 27*, 3, 1–7.

MOUNT, C. M., T. D. B., AND MARSTON, P. L. 1998. Scattering observations for tilted transparent fibers. *Applied Optics 37*, 15341539.

PREMOZE, S., ASHIKHMIN, M., TESENDORF, J., RAMAMOORTHI, R., AND NAYAR, S., 2004. Practical rendering of multiple scattering effects in participating media.

ROBBINS, C. R. 1994. *Chemical and Physical Behavior of Human Hair, third ed.*

STAMM, R. F., GARCIA, M. L., AND J.FUCHS, J. 1977. The optical properties of human hair I. fundamental considerations and goniophotometer curves. *J. Soc. Cosmet. Chem.*, 571–600.

TRICKER, R. A. R., 1970. Introduction to meteorological optics.

ZINKE, A., AND WEBER, A. 2006. Global illumination for fiber based geometries. *SIACG*.

ZINKE, A., AND WEBER, A. 2007. Light scattering from filaments. *Ieee Transactions On Visualization And Computer Graphics*.

ZINKE, A., G., S., AND WEBER, A. 2004. Photo-realistic rendering of blond hair.

ZINKE, A., YUKSEL, C., WEBER, A., AND KEYSER, J. 2008. Dual scattering approximation for fast multiple scattering in hair. In *SIGGRAPH '08: ACM SIGGRAPH 2008 Papers*, ACM, New York, NY, USA.

ZINKE, A. 2007. *Photo-Realistic Rendering of Fiber Assemblies*. PhD thesis, Bonn, Germany. Adviser-Andreas Weber.

A Reflection and Refraction in Cylinders

The loci of the reflections from a cylinder was first introduced to the graphics community by Kajiya and Kay [1989]. They explained that if one considers a parallel beam of light incident to a cylinder, each ray will be reflected across the local surface normal at the intersection point. And since the normals on the cylinders are directed in all directions in the normal plane, the reflected light direction is independent of the azimuthal angle of the incident beam (ϕ_i) and only depends on the longitudinal angle (θ_i). Therefore the reflected distribution of light from a parallel incident beam will lie on a cone with the apex angle equal to the longitudinal angle of the incident beam.

Marschner et al. provided a more mathematical proof for reflections off a smooth cylinder [2003]. They visualized the geometry of the light hitting the hair fiber with a unit sphere (see Figure 40) In this scheme the hair fiber is the vertical diameter of the sphere and normal plane is the horizontal plane which splits the sphere into halves. Assume v_i is the incident angle, local normal is n and the reflected angle is v_r. According to the law of reflection v_i, n and v_r are coplanar and $n.v_i = n.v_t$. In other words the distance of points v_i and v_r to the normal plane is equal. This property holds for any other normal direction, n', as well. Thus, the set of reflections vectors for a given incoming direction v_i is a horizontal circle below the normal plane with the same distance from the normal plane as v_i.

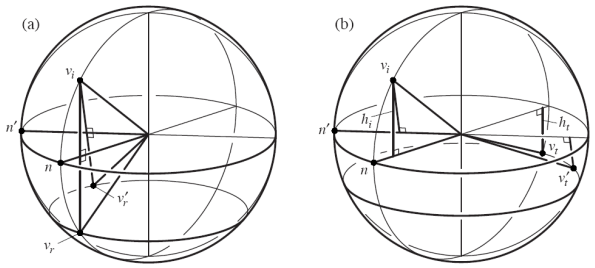

Figure 40: *Geometry of reflection and refraction by a cylinder. (a) Reflected rays. (b) Refracted ray. From [Marschner et al. 2003].*

For investigating the internal reflections inside the cylinder consider Figure 40 b. Snell's Law states that v_i, n and v_t are coplanar and $\eta \sin\theta_t = \sin\theta_i$. Similar discussion implies that the vertical distance of the refracted rays v_t and v_t' to the normal plane is equal. In other words, all the transmitted vectors lie on a horizontal circle below the normal plane. These refracted directions are closer to the normal plane than the incident direction v_i by a factor of η.

Same argument holds for rays which are refracted along the way going out of the cylinder. Beside, multiple internal reflections are similar to external reflections. So, the conclusion is that all the rays that exit a transparent cylinder lie on the same cone which its apex angle is equal to the longitudinal angle of incident beam.

B Bravais Law

Bravais law states that the three dimensional optical analysis of a cylinder can be reduced to the two dimensional analysis of a cross section of the cylinder which contains the surface normal at the point of intersection. However, another effective index of refraction, η', different than the actual refractive index, η should be used in all the calculations. This is valid for any cylindrical fiber with an arbitrary cross section shape. According to this law one can project the incident angle to the normal-plane and apply Snell's law for predicting the amount and direction of reflected and refracted light. The new index of refraction is derived as a function of incident angle. This law is often used in the context of analyzing the optics of crystals. For example, Tricker has used this law to analyze the optics of ice halos [Tricker 1970].

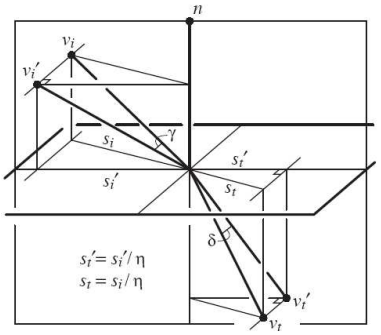

Figure 41: *Derivation of Bravais law. From [Marschner et al. 2003].*

Marschner et al. explained Bravais law by presenting Figure 41. In this figure the incoming light direction is v_i and the refracted light direction is denoted by v_t. Let us project these two directions on to the vertical plane which contains the normal and label them v_i' and

v_t'. We want to find out an effective index of refraction , η', such that it satisfies the Snell's Law for v_i' and v_t'. Note that Snell's Law in 3D states that:

$$\sin\theta_i = \eta \sin\theta_t \tag{46}$$

which means that the projected length of v_i onto the horizontal plane is η times the length of the projection of v_i. One can easily verify that two horizontal triangles in Figure 41 are similar with the similarity ratio of η. The goal is to find η' in the equation $\sin\theta_i' = \eta' \sin\theta_t'$. We have:

$$\sin\theta_i' = \sin\theta_i \cos\gamma \tag{47}$$
$$\sin\theta_t' = \sin\theta_t \cos\delta \tag{48}$$

where γ is the angle between the incident direction and its projection onto the normal plane and similarly, δ is the angle of angle between the refracted direction and its projection to the normal plane. Substitution yields:

$$\sin\theta_i \cos\gamma = \eta' \sin\theta_t \cos\delta \tag{49}$$

and by substituting Equation 46 we will have:

$$\eta \cos\gamma = \eta' cos\delta \tag{50}$$

and finally we get the following expression for calculating η':

$$\eta'(\gamma) = \frac{\sqrt{\eta^2 - \sin^2\gamma}}{\cos\gamma} \tag{51}$$

Bravais law states that after projecting the incident ray to the normal plane, one can use Snell's Law and Fresnel attenuation formulas as usual by using the effective index of refraction η'. For using Fresnel formulas correctly, we still need one more index of refraction η'' which can be derived by the following expression:

$$\eta''(\gamma) = \frac{\eta^2 \cos\gamma}{\sqrt{\eta^2 - \sin^2\gamma}} = \frac{\eta^2}{\eta'(\gamma)} \tag{52}$$

One should use η' for the perpendicular component of the reflectance and η'' for the parallel component. This generalized Fresnel function has been denoted by $F(\eta', \eta'', \gamma)$ [Marschner et al. 2003].